A novel protoapigenone analog RY10-4 induces apoptosis of breast cancer cells by regulating mitochondrial Ca^{2+} influx through the mitochondrial calcium uniporter

Pingping Xue
Huazhong University of Science and Technology
Qian Chen
Huazhong University of Science and Technology
Xiuhua Ren
Huazhong University of Science and Technology
Yimin Yang
Hubei Zhongshan Hospital
Xiaofan Yang (xiaofanyang23@163.com)
Huazhong University of Science and Technology https://orcid.org/0000-0002-0997-0973
Dong Liu
Huazhong University of Science and Technology

Research

Keywords: RY10-4, breast cancer, mitochondrial calcium, MCU, apoptosis

Posted Date: March 13th, 2020

DOI: https://doi.org/10.21203/rs.3.rs-17058/v1

Abstract

Background

Protoapigenone, as a flavonoid compound with a specific nonaromatic B-ring, exhibits extraordinary antitumor activities against a broad spectrum of human cancer cells. Here we developed a novel protoapigenone analog RY10-4, which induces the apoptosis of various tumor cells, especially for breast cancer cells, but the underlying mechanism involved in the apoptotic process remains unclear.

Methods

MTT assay, colony-formation assay and flow cytometry were applied to evaluate the proliferation and apoptosis of breast cancer cells. Cytoplasmic calcium ([Ca2+]c) and mitochondrial calcium ([Ca2+]m) of the breast cancer cells were measured by the Fluo-2 and Rhod-2 probes, respectively. The mitochondrial reactive oxygen species (mtROS), membrane potential (ΔΨm) and permeability transition pore (mPTP) were analyzed by MitoSOX, JC-1 probes and Calcein/AM, respectively. Furthermore, Western bolt assay was adopted for the exploration of the mitochondrial apoptosis pathway. Besides, the xenograft assay was performed to investigate the role of RY10-4 in breast cancer cells in vivo.

Results

Obviously, RY10-4 could effectively suppress the proliferation and induce the apoptosis of breast cancer cells. Furthermore, the [Ca2+]c and [Ca2+]m of MDA-MB-231 cells were up-regulated after the treatment of RY10-4, resulting in the mtROS accumulation, ΔΨm depolarization and mPTP opening. And finally, the mitochondrial apoptosis was activated by the release of cytochrome C. Interestingly, the inhibition of mitochondrial calcium uniporter (MCU) with Ru360 attenuated the overload of [Ca2+]m and blocked the apoptosis of MDA-MB-231 cells induced by RY10-4, which was also consistent with the in vivo results.

Conclusions

From the results we concluded that RY10-4 could induce apoptosis of breast cancer cells by elevating [Ca2+]m through MCU. Our work contributed previously unknown insights into the mechanisms involving in the clinical efficacy of RY10-4 on breast cancer cells, which also advanced calcium homeostasis as a potential target for chemotherapeutic drugs.

Background

Breast cancer, ranked as the top five most frequently diagnosed cancers, has developed as the most threatening health issue for women due to its high incidence and mortality all over the world [1]. For the treatments of breast cancer, a variety of therapeutic methods have been developed, including surgical operation, radiotherapy, endocrinotherapy and chemotherapy [2, 3]. Although the combination of surgery with radiotherapy and/or chemotherapy has been broadly employed as the therapy of breast cancer, the subsequent metastasis and recurrence also result in the high mortality related to breast cancer [4, 5].

Besides, side effects and drug resistance often happen in the chemotherapy for breast cancer, which limit the therapeutic effects in practice [6, 7]. Consequently, it is of great necessity to develop novel treatments for improving the efficacy of breast cancer therapy.

So far, more and more attention has been aroused to the medicinal value of traditional Chinese medicine due to its acknowledged safety and therapeutic effects for breast cancer [8, 9]. The compounds extracted from plants and the ones designed on account of plant-derived compounds have been proved as excellent novel chemotherapeutic drugs [10, 11]. Protoapigenone, belonging to the flavonoid with a specific nonaromatic B-ring, plays a dramatically cytotoxic role in cells, which has been considered as the promising compound for anticancer drug development [12, 13]. On account of protoapigenone and its relevant flavonoids, we have designed and successfully synthesized the derivative, RY10-4 (Fig. 1), which displays intensifying cytotoxic effects on cancer cells (especially for breast cancer cells) and a reduced impact on normal cells [14]. Nevertheless, the potential mechanisms on the apoptotic process of breast cancer cells remain indistinct and need to be further interpreted.

As a crucial intracellular signal molecule, Ca^{2+} plays a role in the modulations of various cellular functions, including energy generation, cell growth and cell proliferation [15, 16]. Nevertheless, compared with the beneficial impacts, several adverse effects can be induced by Ca^{2+} in terms of the mitochondrial function, which also trigger cell death via either necrosis or apoptosis [17, 18]. The homeostasis of $[Ca^{2+}]m$ is of great importance for regulating the aerobic metabolism and cell viability, whereas the overload of $[Ca^{2+}]m$ is fatal to cells. It is acknowledged that the up-regulated Ca^{2+} in the mitochondrial matrix contributes to the elevated synthesis of reactive oxygen species, the opening of permeability transition pore (mPTP), and the release of cytochrome C, which finally trigger the cell apoptosis [19]. $[Ca^{2+}]m$ uptake is achieved primarily through MCU, which displays highly Ca^{2+} selectivity ($Kd < 2$ nM) and pharmacological sensitivity to ruthenium red (RR) [20].

In our work, excessive accumulation of Ca^{2+} in mitochondria was identified in the breast cancer cells after the RY10-4 treatment, further leading to mtROS accumulation, $\Delta\Psi m$ depolarization, mPTP opening and final apoptosis. To investigate the role of MCU in RY10-4 induced breast cancer cells apoptosis, the MCU inhibitor Ru360 was adopted to block the mitochondrial Ca^{2+} influx, which relieved the overload of mitochondrial Ca^{2+}, improved the mitochondrial function and inhibited the apoptosis of breast cancer cells. Xenograft assay was subsequently performed to confirm the in vivo effect of RY10-4 on breast cancer cells. Obvious suppression of tumor growth was identified in the RY10-4-treated group, which was also reversed by the Ru360 treatment. Taken together, the present study confirmed the inhibitory effect of RY10-4 on breast cancer, which was attributed to the MCU-mediated mitochondrial calcium overload.

Methods

Cell culture and treatment

MDA-MB-231, MCF-7 and SKBR-3 human breast cancer cell lines and MCF-10A normal human breast epithelial cell line were acquired from Tongji hospital, Wuhan, China. The MDA-MB-231, MCF-7 and SKBR3 cells were cultured in the RPMI-1640 (Boster, China) culture medium with 10% (v/v) fetal bovine serum (FBS; Gibco, USA), 100 U/mL penicillin and 100 μg/mL streptomycin. Comparatively, MCF-10A cells were cultivated in the DMEM/F12 (Boster) culture medium with 5% (v/v) horse serum, 20 ng/mL EGF, 0.5 mg/mL Hydrocortisone, 100 ng/mL Cholera Toxin, 10 μg/mL Insulin, 100 U/mL penicillin and 100 μg/mL streptomycin. All the cells were cultured at 37 °C with 5% CO_2.

RY10-4 was designed and synthesized by Yuan et al. as previously described(14) and dispersed in dimethyl sulfoxide (DMSO) to obtain a 10 μM stock solution. A concentration gradient of RY10-4 were administrated to cells for 24 h to investigate the inhibitory effect on breast cancer cells. To explore the role of MCU in mitochondrial Ca^{2+} uptake, cells were pretreated with 10 μM Ru360 (MCU inhibitor; Sigma-Aldrich, USA) and 10 μM spermine (MCU agonist; Topscience, China) for 30 min before the RY10-4 administration. The calcium chelator, BAPTA-AM, (1 μM; Topscience) was applied to maintain the intracellular Ca^{2+} levels.

MTT assay

MTT assay was conducted as formerly indicated [21]. Briefly, each well of a 96-well culture plate was seeded with 5×10^3 cells and cultured overnight, which were subsequently cultured in the fresh culture medium with various concentrations of RY10-4 for additional 24 h. For the cell survival detection, 0.2 mL MTT (Sigma-Aldrich) was administrated to each well and was further incubated for 2 h. After dissolution with 0.2 mL DMSO, the microplate reader (Bio-Rad Laboratories, USA) was employed to identify the optical density (O.D.) of the supernatant. The ratio of survived cells was regarded as the O.D. value of the sample compared with the control group.

Plate clone formation assay

Cells were seeded in 6-well plates with the density of 1000 cells/well and administrated with various concentrations of RY10-4. Medium was discarded and replaced after incubating for 24 h and cells were further observed for another 7 days. Colonies were rinsed with PBS, fixed in the 4% polyformaldehyde for 20 min, which were treated with 1% Crystal Violet Staining Solution (Beyotime, China) for 20 min after the removal of fixing solution. Eventually, the microscope was adopted for the counting of colonies in each well.

Apoptosis evaluation by flow cytometry

MDA-MB-231 cells, in the logarithmic phase, were cultured in 6-well plates with the density of 2×10^5 cells/well, followed by the administration of RY10-4, Ru360, Spermine or BAPTA for 24 h. Subsequently, the cells were resuspended in the Annexin V and propidium iodide (PI) binding buffer and cultured for 15 min at 37 °C in the dark. The FACS Calibur flow cytometer (Bectone Dickinson, USA) was employed for further analysis. Cells were regarded as apoptotic when the annexin V was positive and PI negative, while the double-positive cells were either necrosis or late apoptosis.

Cytoplasmic and mitochondrial Ca^{2+} assay

To measure the levels of $[Ca^{2+}]c$ and $[Ca^{2+}]m$, the MDA-MB-231 cells were incubated with Fluo-2 and Rhod-2 (Thermo Fisher Scientific, USA) for 30 min at 37 °C in accordance with the manufacturer's instructions. The fluorescence of Fluo-2 and Rhod-2 were visualized by a confocal laser scanning microscope (Carl Zeiss, Germany) at the excitation of 340 and 550 nm, and emission of 500 and 570 nm, respectively.

mtROS measurement

To measure the mtROS formation, MDA-MB-231 cells were labeled with MitoSOX Red (Thermo Fisher Scientific), a highly selective fluorescent probe, for the detection of $O_2^{\bullet -}$ generated within mitochondria. Briefly, cells were cultured in a cell culture dish and were treated as indicated. MitoSOX Red reagent stock solution was diluted in HBSS/Ca/Mg buffer to generate a 5 μM reagent working solution. Cells were then incubated with 5 μM MitoSOX Red reagent working solution in the dark at 37 °C for 10 min. After three washes with warm buffer, live imaging was performed using a confocal laser scanning microscope. The results were obtained from at least 30 cells in each group.

Evaluation of mPTP opening

The mPTP opening was confirmed by co-loading cells with Calcein/AM (Solarbio, China) and $CoCl_2$ (Sigma-Aldrich) based on the former researches [22]. Briefly, MDA-MB-231 cells were cultured with 2 μM Calcein/AM and 1 mM $CoCl_2$ at room temperature for 35 min, followed by rinsing with 1 mM $CoCl_2$ for 25 min. Subsequently, the confocal laser scanning microscope was applied to monitor the calcein fluorescence at ex/em wavelengths of 488/515 nm. The loss of fluorescence was considered as an index for mPTP opening.

Detection of ΔΨm

ΔΨm was analyzed in the MDA-MB-231 cells via the JC-1 probe (Beyotime). Cells were primarily treated with the JC-1 staining solution for 20 min at 37 °C, which were visualized by the confocal laser scanning microscopy. Ulteriorly, the Zeiss LSM Image Examiner software was applied to quantify the intensities of red and green fluorescence, which referred to the aggregate and monomeric form of JC-1, respectively. The ratio of the intensity of red fluorescence to that of green was regarded as ΔΨm. For each group, at least 30 cells were measured.

Western blot

Cells were collected and protein extraction was carried out as described previously [23]. Mitochondria were isolated from the MDA-MB-231 cells or tumors by the Mitochondria Isolation Kits (Solarbio) based on the instructions of manufacturer. The level of protein was identified based on the BCA method, and equivalent amounts of samples were loaded on 10% SDS–PAGE followed by transferring onto the nitrocellulose membrane. Membranes were blocked with 5% milk for 1 h and further incubated overnight with the primary antibodies as follows: rabbit anti-Bax (1:5000; Abcam, UK), rabbit anti-Bcl-2 (1:2000;

Abcam), rabbit anti-cleaved-caspase 9 (1:1000; Cell Signaling Technology, USA), rabbit anti-cleaved-caspase 3 (1:2000; Cell Signaling Technology), rabbit anti-cytochrome C (1:5000; Abcam), mouse anti-GAPDH (1:5000; Proteintech, China) and rabbit anti-COX IV (1:1000; Proteintech). Subsequently, the above membranes were treated with the HRP-conjugated secondary antibody (1:5000; Santa Cruz Biotech) for 1 h, and immunoreactivity was detected with the ECL system, the images of which were analyzed with Quantity One (Bio-Rad, USA). The Western blot assay of MDA-MB-231 tumors were similarly performed as above mentioned.

In vivo toxicity assessment of RY10-4

Five-week old male C57BL/6J mice were obtained from the Animal Experiment Center of Huazhong University of Science and Technology and cultivated in the constant laboratory conditions with a 12 h light/dark cycle. After the acclimatization, mice were randomly separated to two groups (5 for the RY10-4 treatment group and 5 for the control group). Mice of the RY10-4 treatment group were intraperitoneally injected with RY10-4 (15 mg/kg) every other day for 65 consecutive days, while those of the control group were injected with equal volume of PBS intraperitoneally. Mice were weighted every five days and the urine was collected for urinalysis by Bradford Protein Assay. Afterwards, the mice were sacrificed and their organs (hearts, kidneys, livers and lungs) were collected for histological analysis.

Hematoxylin & eosin (H & E) staining

For the HE staining assay, 4% paraformaldehyde was adopted for the fixing of samples, followed by dehydration and embedding with paraffin. Cross-sectional slices of the muscle tissues with the thickness of 4 μm were prepared and stained with HE staining solution (Bioyear, China) to perform the histological analysis.

Xenograft assay

MDA-MB-231 cells (2×10^6 cells/mouse) in 0.2 mL culture medium were subcutaneously implanted in the right armpit of female BALB/c-nu mice (4 weeks old; Hunan SJA Laboratory Animal Co. Ltd., China). Tumor growth was recorded every 3 days when the diameter of subcutaneous tumors reached 0.3 cm. Mice were randomly separated to the following groups (n = 5 per group): control group (normal saline), RY10-4 (15 mg/kg) group, RY10-4 (15 mg/kg) + Ru360 (50 nmol/kg) group and RY10-4 (15 mg/kg) + spermine (5 mg/kg) group. All the mice were intraperitoneally injected with corresponding solutions every other day for 3 consecutive weeks. Tumor volumes were calculated according to the formula below: Tumor volume = $ab^2/2$ (where a represented for the long diameter and b for the short diameter of the tumor). The relative tumor volume (RTV) was further calculated as the ratio of the tumor volume at each time point (V_t) and that before the systemic administration (V_0). 3 weeks later, all the mice were sacrificed and the subcutaneous tumors were obtained and weighted. All experimental procedures were in accordance with the guidelines of the Chinese National Institutes of Health, and the experimental protocols were authorized by the Ethical Committee on Animal Experiments (Huazhong University of Science and Technology).

Immunohistochemical staining assay

The embedded tissue sections were treated with primary rabbit polyclonal antibodies against Bax (1:500), Bcl-2 (1:500) and cleaved-caspase 3 (1:250), followed by incubating with horseradish peroxidase-conjugated secondary antibodies (1:200). Eventually, 3,3'-diaminobenzidine (DAB) (Boster) was applied for the immunohistochemistry staining.

Statistical analysis

The GraphPad Prism 5 software (GraphPad Software, USA) was applied for data analyses. Data were independently collected for three times, which were expressed as mean ± standard deviation (SD) and compared based on the ANOVA with a post-hoc Dunnett's test. $P < 0.05$ was considered as statistically significant.

Results

RY10-4 restrained proliferation and induced apoptosis of breast cancer cells

To verify the inhibitory role of RY10-4 in breast cancer cells, three breast cancer cell lines (HER2-/ER-: MDA-MB-231; HER2-/ER+: MCF-7; HER2+/ER-: SKBR3) and normal human breast epithelial cells MCF-10A were selected in this study. The MTT assay revealed that RY10-4 could significantly downregulate the cell viability of all the three breast cancer cell lines in a concentration dependent manner (approximately 60–80% reduction was achieved at the RY10-4 concentration of 2.5 μM), while the suppressive effect on MCF-10A cells was much milder (Fig. 2A). Similar results were also observed in the plate clone formation assay, in which RY10-4 markedly disrupted colony formation in the breast cancer cell lines and exerted much weaker impacts on MCF-10A (Fig. 2B). The above results confirmed the selective antiproliferation effect of RY10-4 on breast cancer cells. The MDA-MB-231 cells, which were the most inhibited in MTT and clone formation assay, were chosen for the next experiments. Further, the role of RY10-4 in the apoptosis of breast cancer cells was investigated based on flow cytometry. Obviously, the apoptosis of MDA-MB-231 cells were markedly induced by RY10-4 in a concentration dependent manner with the apoptosis rate of 37.43 ± 2.32% at 2.5 μM (Fig. 3). In short, it was indicated that RY10-4 could restrain cell proliferation and trigger the apoptosis of breast cancer cells.

RY10-4 induced mitochondria Ca^{2+} overload and dysfunction in breast cancer cells

To interpret the mechanism of RY10-4 induced apoptosis, calcium homeostasis and mitochondrial function were evaluated. As expected, both the $[Ca^{2+}]c$ and $[Ca^{2+}]m$ in MDA-MB-231 cells were

predominantly elevated by RY10-4, which were visualized by Fluo-2 and Rhod-2 probes, respectively (Fig. 4).

Since ROS was primarily produced in the mitochondria, the dysfunction of mitochondria with inhibited activities of the mitochondrial respiratory chain complexes contributed to the overproduced mtROS [24]. Here the mtROS levels in the MDA-MB-231 cells were accessed by MitoSOX Red, and it was demonstrated that the RY10-4 treatment predominantly upregulated the production of mtROS (Fig. 5A and D).

ΔΨm, which was of great necessity for the oxidative phosphorylation and ATP production in mitochondria [25], was also explored in MDA-MB-231 cells. In accordance with the results of mtROS, the ratio of intensities of red to green fluorescence was dramatically down-regulated by RY10-4, suggesting the depolarization of ΔΨm (Fig. 5B and E).

As a non-selective channel, mPTP allowed the passage of molecules up to 1.5 kDa. It was well acknowledged for its pathological effect on the modulation of mitochondrial dysfunction and apoptosis [26]. As revealed before, RY10-4 treatment was also able to promote the opening of mPTP in MDA-MB-231 cells (Fig. 5C and F).

In brief, the above results indicated that RY10-4 induced mitochondria Ca^{2+} overload and dysfunction in breast cancer cells.

Inhibition of MCU blocked the mitochondria Ca $^{2+}$ uptake, improved mitochondria function and reversed RY10-4 induced apoptosis in breast cancer cells

Considering the vital role of MCU in mitochondrial Ca^{2+} influx, we speculated that the RY10-4-induced inhibitory effect on breast cancer cells could be attenuated by suppressed MCU. Here the MCU inhibitor, Ru360, was adopted to block the influx of mitochondrial Ca^{2+}, and it was indicated that the RY10-4 induced $[Ca^{2+}]$m overload was almost eliminated by Ru360, similar to the activity of BAPTA as an intracellular calcium chelator. Conversely, the treatment with the MCU agonist spermine exhibited no distinct difference with the single use of RY10-4 (Fig. 4). Additionally, the overproduction of mtROS induced by RY10-4 was notably down-regulated by Ru360, accomplished by restoring ΔΨm and preventing mPTP opening (Fig. 5).

In view of the effect of mPTP on the mitochondrial apoptosis, the expressions of proteins involved in the apoptosis signaling pathway were determined. As displayed in Fig. 6, the pro-apoptotic cleaved caspase-3, cleaved caspase-9, and Bax were markedly up-regulated and anti-apoptotic Bcl-2 were down-regulated after the RY10-4 treatment. The treatment of Ru360 blocked the signaling pathway, which was in consistent with the results of BAPTA. As expected, there were no conspicuous differences between the results of spermine treatment and those of the single use of RY10-4. Characterized by the release of

cytochrome C from mitochondria to cytoplasm [27], the mitochondrial apoptosis was evaluated by measuring the levels of cytochrome C in cytosol and mitochondria respectively. In accordance with previous researches, the levels of cytochrome C in cytosol were elevated and those in mitochondria were decreased after the treatment of RY10-4 in MDA-MB-231 cells, while the administration of Ru360 or BAPTA neutralized the effect of RY10-4. Spermine treated MDA-MB-231 cells exhibited similar cytochrome C expression behaviors to the RY10-4 treated cells. Eventually, the flow cytometry analysis of apoptosis was performed to identify the role of MCU in the apoptosis f MDA-MB-231 cells. As with former results, the treatments of Ru360 and BAPTA dramatically reduced the apoptosis rate compared to the single use of RY10-4, while the administration of spermine increased the apoptosis rate in contrast to the single RY10-4 treatment (Fig. 3). Totally, the above results demonstrated that the MCU dependent mitochondrial Ca^{2+} influx impaired the mitochondria function and mediated the apoptosis of breast cancer cells induced by RY10-4.

RY10-4 was well tolerated in mouse models

As discussed above, the in-vitro studies proved that RY10-4 induced selective apoptosis in cancer cells, thus distinguishing between cancerous and non-cancerous cells. Accordingly, the safety of RY10-4 was further determined in vivo. Here we assessed the safety of systemic RY10-4 treatment in normal C57BL/6J mice, at a dose of 15 mg/kg every other day for 65 consecutive days. The mice were constantly monitored for any indications of toxicity based on weight measurement and protein urinalysis. No conspicuous differences of weight or urinary protein were observed between the control group and the RY10-4-induced group, suggesting the hypotoxicity of RY10-4 (Fig. 7A and B). Limited urinary protein of mice in each group were identified without remarkable differences between groups.

After the completion of in vivo research, relevant organs were obtained from mice for histopathological analysis. HE staining of the hearts, kidneys, livers and lungs showed no gross morphological differences between the control and the RY10-4 treated groups (Fig. 7C). The tissue lesions were minimal or mild and were interpreted as either background or incidental and none was of a type or frequency indicative of RY10-4 toxicity to the C57BL/6J mice. In summary, the safety of the systemic administration of RY10-4 was confirmed in the mouse models based on the above data.

RY10-4 retarded the growth of breast tumors, which was reversed by MCU inhibitor in mouse xenograft models

To further investigate the antitumor activities of RY10-4 in vivo, the nude mice xenografts of breast cancer were developed and the tumors were excised for the analysis after administration. The results demonstrated that the single use of RY10-4 and its combination with spermine markedly suppressed the growth of MDA-MB-231 tumors, showing a much lower tumor weight and volume than the control group. However, the administration of Ru360 nearly reversed the inhibitory effect of RY10-4 on the MDA-MB-231 tumors (Fig. 8A-C). Furthermore, immunohistochemical staining and western blot were performed to

explore the mitochondrial apoptosis pathway. Similar to the in vitro results, RY10-4 induced the upregulation of proapoptotic proteins, downregulation of antiapoptotic protein and the release of cytochrome C from mitochondria to cytoplasm, which could be inhibited by the Ru360 treatment (Fig. 8D and E). To sum up, it was indicated that RY10-4 could retard the growth of breast tumors by the mitochondria apoptosis pathway via MCU.

Discussion

Plant extracts are widely known as the promising source for drug discovery, which plays a crucial role in discovering and designing novel chemotherapeutic agents [28, 29]. As a natural flavonoid derived from plants, protoapigenone, with a specific nonaromatic B-ring, exhibits remarkable cytotoxic activity, which has been served as the leading agent for developing novel anticancer drugs. On account of the structure of protoapigenone and its relevant flavonoids, we have successfully designed and synthesized the novel compound RY10-4 [14]. Interestingly, RY10-4 displayed enhanced cytotoxicity in cancer cells and decreased cytotoxicity in normal cells, which was consistent with the results in Fig. 2. However, despite its definite antitumor effect, the scientific research focused on the underlying mechanism is still limited.

In the present study, we evaluated the anti-tumor activity of RY10-4 in breast cancer. The results showed that RY10-4 effectively inhibited proliferation and induced apoptosis of MDA-MB-231, MCF-7 and SKBR-3 cells. Furthermore, xenograft assay was performed to determine the in vivo effects of RY10-4 on breast cancer, yielding similar results. Briefly, these results revealed a concentration-dependent inhibition effect of RY10-4 on breast cancer, indicating its potential in clinical application.

Ca^{2+} is a major second messenger in cellular signaling regulating muscle contraction, neuronal excitability, cell migration, and proliferation [16]. In order to maintain a delicate regulation of Ca^{2+} homeostasis, various plasma membrane and organellar Ca^{2+} channels, exchangers and transporters are needed. The majority of intracellular Ca^{2+} is stored in the endoplasmic or sarcoplasmic reticulum (ER/SR) [30]. However, it is also known that the dynamic organelles such as the mitochondria can play a major role in buffering and shaping the cytosolic Ca^{2+} [31, 32]. The influx of Ca^{2+} into mitochondria is primarily mediated by MCU, which is a mitochondrial Ca^{2+} channel and plays a fundamental role in mediating global calcium signaling. The transport of Ca^{2+} cations into the mitochondrial matrix is vital for the mitochondrial function, such as the tricarboxylic acid cycle (TCA), adenosine triphosphate (ATP) production, and ROS generation [24]. However, excessive $[Ca^{2+}]m$ is also able to determine cell fate, since the overload of mitochondrial Ca^{2+} can elevate mtROS, induce $\Delta\Psi m$ depolarization and promote mPTP opening, which subsequently activate the mitochondrial apoptosis. Indeed, we found the overload of $[Ca^{2+}]c$ and $[Ca^{2+}]m$ in RY10-4 treated breast cancer cells, which further disrupted the mitochondrial functions (characterized by mtROS overproduction, $\Delta\Psi m$ depolarization and mPTP opening as revealed in Fig. 5) and induced cell apoptosis. To clarify the process of mitochondrial Ca^{2+} influx, the MCU inhibitor Ru360 was administrated to the cell culture, which subsequently relieved the $[Ca^{2+}]m$ overload, improved the mitochondrial function and inhibited the RY10-4 induced apoptosis. These results

confirmed the core role of Ca^{2+} homeostasis and mitochondrial function in the antitumor activity of RY10-4.

The ability to inhibit apoptosis and resist cell death is one of the well-established hallmarks of cancer [33]. Ca^{2+} and mtROS, as the cell death inducers, are tightly regulated by mitochondria to maintain cell homeostasis [24]. While in breast cancer cells, $[Ca^{2+}]$m overload and mtROS overproduction were achieved by RY10-4 treatment, which was able to further activate the mitochondrial apoptosis. As expected, we consistently observed the increase of apoptosis in RY10-4 treated breast cancer cells and tumors (shown in Figs. 3 and 8). Besides, the expression variations of apoptotic regulators in mitochondrial apoptosis were also explored by western blot, showing a consistent trend as described in previous studies [34]. To be detailed, the anti-apoptotic Bcl-2 family proteins such as Bcl-2 and Bcl-xl were displaced upon activation, permitting the pro-apoptotic Bax and Bcl-2 antagonist/killer 1 (Bak) to translocate to the outer mitochondrial membrane (OMM) and regulate OMM permeabilization. This was followed rapidly by the pore formation, and subsequent release of the mitochondria-resided apoptogenic factors (e.g. cytochrome c, AIF and Smac/DIABLO) into the cytosol. Subsequently, caspase-9 mediated apoptosis by assembling an apoptosome complex through the interaction of procaspase-9 with Apaf-1, dATP/ATP, and mitochondrial released cytochrome c, which subsequently recruited procaspase-3 to the complex and efficiently activated caspase-3, a common effector caspase, by the caspase-9-mediated proteolytic cleavage and finally resulted in cell apoptosis [35, 36].

Since ER-mitochondria transfer accounts largely for mitochondrial Ca^{2+} uptake and its alterations play a crucial role in cancer progression [37, 38], it is necessary to explore the upstream mechanism for ER Ca^{2+} release or the possible endoplasmic reticulum stress in our future research. Besides, the quantitative analysis of MCU and its regulators including mitochondrial calcium uptake 1 (MICU1), mitochondrial calcium uptake 2 (MICU2) and mitochondrial calcium uniporter regulator 1 (MCUR1) [39] were not involved in the present research considering the complexity and uncertainty therein, which will be taken into consideration in our next work.

Conclusions

To summarize, the present study confirmed the inhibitory effect of RY10-4 on breast cancer cells, in which the MCU dependent mitochondrial Ca^{2+} influx accounted for the mitochondrial dysfunction and apoptosis. These findings interpreted the previously unknown insights into the mechanisms in the antitumor effect of RY10-4 and revealed the potential of RY10-4 to be developed as a chemotherapeutic agent for breast cancer.

Abbreviations

$[Ca^{2+}]$c: cytoplasmic calcium; $[Ca^{2+}]$m: mitochondrial calcium; ΔΨm: mitochondrial membrane potential; mPTP: mitochondrial permeability transition pore; MCU: mitochondrial calcium uniporter; RR: ruthenium red; FBS: fetal bovine serum; DMSO: dimethyl sulfoxide; PI: propidium iodide; RTV: relative tumor volume;

mtROS: mitochondrial reactive oxygen species; ER: endoplasmic reticulum; TCA: tricarboxylic acid cycle; ATP: adenosine triphosphate; Bak: Bcl-2 antagonist/killer; OMM: outer mitochondrial membrane; MICU1: mitochondrial calcium uptake 1; MICU2: mitochondrial calcium uptake 2; MCUR1: mitochondrial calcium uniporter regulator 1.

Declarations

Acknowledgements

We kindly thank the Science Foundation of Tongji Hospital for the funding.

Availability of data and material

All data generated in this study are included in the manuscript.

Funding

This work was supported by the Science Foundation of Tongji Hospital (Grant number 2201300801).

Authors' contributions

XFY and DL designed the conceptual idea for this study. PPX performed most of the experiments. QC and XHR established the mouse model. YMY conducted the mice feed and tumor volume measurement. PPX and XFY wrote the manuscript. All the authors approved the submission of this manuscript in its final form.

Ethics approval

Ethical approval to conduct the study was obtained from the Ethical Committee on Animal Experiments of Huazhong University of Science and Technology.

Consent for publication

All the authors give their consent for publication.

Competing interests

The authors declare that they have no competing interests.

References

1. Bray F, Ferlay J, Soerjomataram I, Siegel RL, Torre LA, Jemal A. Global cancer statistics 2018: globocan estimates of incidence and mortality worldwide for 36 cancers in 185 countries. CA Cancer J Clin. 2018;68(6):394-424.

2. Nunez C, Capelo JL, Igrejas G, Alfonso A, Botana LM, Lodeiro C. An overview of the effective combination therapies for the treatment of breast cancer. BIOMATERIALS. 2016;97:34-50.
3. Anampa J, Makower D, Sparano JA. Progress in adjuvant chemotherapy for breast cancer: an overview. BMC MED. 2015;13:195.
4. Long-term outcomes for neoadjuvant versus adjuvant chemotherapy in early breast cancer: meta-analysis of individual patient data from ten randomised trials. LANCET ONCOL. 2018;19(1):27-39.
5. Dittmer J. Mechanisms governing metastatic dormancy in breast cancer. SEMIN CANCER BIOL. 2017;44:72-82.
6. Chambers CS, Viktorova J, Rehorova K, Biedermann D, Turkova L, Macek T, Kren V, Valentova K. Defying multidrug resistance! Modulation of related transporters by flavonoids and flavonolignans. J Agric Food Chem. 2020;68(7):1763-1779.
7. Dallavalle S, Dobricic V, Lazzarato L, Gazzano E, Machuqueiro M, Pajeva I, Tsakovska I, Zidar N, Fruttero R. Improvement of conventional anti-cancer drugs as new tools against multidrug resistant tumors. Drug Resist Updat. 2020;50:100682.
8. Wang D, Huang J, Gui T, Yang Y, Feng T, Tzvetkov NT, Xu T, Gai Z, Zhou Y, Zhang J et al. Sr-bi as a target of natural products and its significance in cancer. SEMIN CANCER BIOL. 2020.
9. Sun X, Yan P, Zou C, Wong YK, Shu Y, Lee YM, Zhang C, Yang ND, Wang J, Zhang J. Targeting autophagy enhances the anticancer effect of artemisinin and its derivatives. MED RES REV. 2019;39(6):2172-2193.
10. Efferth T, Saeed M, Kadioglu O, Seo EJ, Shirooie S, Mbaveng AT, Nabavi SM, Kuete V. Collateral sensitivity of natural products in drug-resistant cancer cells. BIOTECHNOL ADV. 2020;38.
11. Efferth T, Oesch F. Repurposing of plant alkaloids for cancer therapy: pharmacology and toxicology. SEMIN CANCER BIOL. 2019.
12. Lin AS, Chang FR, Wu CC, Liaw CC, Wu YC. New cytotoxic flavonoids from thelypteris torresiana. PLANTA MED. 2005;71(9):867-870.
13. Huang XH, Xiong PC, Xiong CM, Cai YL, Wei AH, Wang JP, Liang XF, Ruan JL. In vitro and in vivo antitumor activity of macrothelypteris torresiana and its acute/subacute oral toxicity. PHYTOMEDICINE. 2010;17(12):930-934.
14. Yuan Q, Liu Z, Xiong C, Wu L, Wang J, Ruan J. A novel, broad-spectrum antitumor compound containing the 1-hydroxycyclohexa-2,5-dien-4-one group: the disclosure of a new antitumor pharmacophore in protoapigenone 1. BIOORG MED CHEM LETT. 2011;21(11):3427-3430.
15. Xu H, Fang T, Yan H, Jiang L. The protein kinase cmk2 negatively regulates the calcium/calcineurin signalling pathway and expression of calcium pump genes pmr1 and pmc1 in budding yeast. CELL COMMUN SIGNAL. 2019;17(1):7.
16. Bagur R, Hajnoczky G. Intracellular Ca^{2+} sensing: its role in calcium homeostasis and signaling. MOL CELL. 2017;66(6):780-788.

17. Orrenius S, Zhivotovsky B, Nicotera P. Regulation of cell death: the calcium-apoptosis link. Nat Rev Mol Cell Biol. 2003;4(7):552-565.
18. Finkel T, Menazza S, Holmstrom KM, Parks RJ, Liu J, Sun J, Liu J, Pan X, Murphy E. The ins and outs of mitochondrial calcium. CIRC RES. 2015;116(11):1810-1819.
19. Pathak T, Trebak M. Mitochondrial Ca^{2+} signaling. Pharmacol Ther. 2018;192:112-123.
20. Gutierrez T, Parra V, Troncoso R, Pennanen C, Contreras-Ferrat A, Vasquez-Trincado C, Morales PE, Lopez-Crisosto C, Sotomayor-Flores C, Chiong M et al. Alteration in mitochondrial Ca^{2+} uptake disrupts insulin signaling in hypertrophic cardiomyocytes. CELL COMMUN SIGNAL. 2014;12:68.
21. Luo Z, Hu X, Xiong H, Qiu H, Yuan X, Zhu F, Wang Y, Zou Y. A polysaccharide from huaier induced apoptosis in mcf-7 breast cancer cells via down-regulation of mtdh protein. Carbohydr Polym. 2016;151:1027-1033.
22. Kar D, Bandyopadhyay A. Targeting peroxisome proliferator activated receptor alpha (ppar alpha) for the prevention of mitochondrial impairment and hypertrophy in cardiomyocytes. CELL PHYSIOL BIOCHEM. 2018;49(1):245-259.
23. Yang X, Xue P, Liu X, Xu X, Chen Z. Hmgb1/autophagy pathway mediates the atrophic effect of tgf-beta1 in denervated skeletal muscle. CELL COMMUN SIGNAL. 2018;16(1):97.
24. Bertero E, Maack C. Calcium signaling and reactive oxygen species in mitochondria. CIRC RES. 2018;122(10):1460-1478.
25. Demine S, Renard P, Arnould T. Mitochondrial uncoupling: a key controller of biological processes in physiology and diseases. CELLS-BASEL. 2019;8(8).
26. Bernardi P, Rasola A, Forte M, Lippe G. The mitochondrial permeability transition pore: channel formation by f-atp synthase, integration in signal transduction, and role in pathophysiology. PHYSIOL REV. 2015;95(4):1111-1155.
27. Hafsia N, Forien M, Renaudin F, Delacour D, Reboul P, Van Lent P, Cohen-Solal M, Liote F, Poirier F, Ea HK. Galectin 3 deficiency alters chondrocyte primary cilium formation and exacerbates cartilage destruction via mitochondrial apoptosis. INT J MOL SCI. 2020;21(4).
28. Weng W, Goel A. Curcumin and colorectal cancer: an update and current perspective on this natural medicine. SEMIN CANCER BIOL. 2020.
29. Gupta B, Sadaria D, Warrier VU, Kirtonia A, Kant R, Awasthi A, Baligar P, Pal JK, Yuba E, Sethi G et al. Plant lectins and their usage in preparing targeted nanovaccines for cancer immunotherapy. SEMIN CANCER BIOL. 2020.
30. Padamsey Z, Foster WJ, Emptage NJ. Intracellular Ca^{2+} release and synaptic plasticity: a tale of many stores. NEUROSCIENTIST. 2019;25(3):208-226.
31. Kerkhofs M, Bultynck G, Vervliet T, Monaco G. Therapeutic implications of novel peptides targeting er-mitochondria Ca^{2+}-flux systems. DRUG DISCOV TODAY. 2019;24(5):1092-1103.
32. Giorgi C, Marchi S, Pinton P. The machineries, regulation and cellular functions of mitochondrial calcium. Nat Rev Mol Cell Biol. 2018;19(11):713-730.

33. Diederich M, Cerella C. Non-canonical programmed cell death mechanisms triggered by natural compounds. SEMIN CANCER BIOL. 2016;40-41:4-34.
34. Yang X, Xue P, Chen H, Yuan M, Kang Y, Duscher D, Machens HG, Chen Z. Denervation drives skeletal muscle atrophy and induces mitochondrial dysfunction, mitophagy and apoptosis via mir-142a-5p/mfn1 axis. THERANOSTICS. 2020;10(3):1415-1432.
35. Fletcher L, Nabrinsky E, Liu T, Danilov A. Cell death pathways in lymphoid malignancies. CURR ONCOL REP. 2020;22(1):10.
36. Bock FJ, Tait S. Mitochondria as multifaceted regulators of cell death. Nat Rev Mol Cell Biol. 2020;21(2):85-100.
37. Raffaello A, Mammucari C, Gherardi G, Rizzuto R. Calcium at the center of cell signaling: interplay between endoplasmic reticulum, mitochondria, and lysosomes. TRENDS BIOCHEM SCI. 2016;41(12):1035-1049.
38. Phillips MJ, Voeltz GK. Structure and function of er membrane contact sites with other organelles. Nat Rev Mol Cell Biol. 2016;17(2):69-82.
39. Williams GS, Boyman L, Chikando AC, Khairallah RJ, Lederer WJ. Mitochondrial calcium uptake. Proc Natl Acad Sci U S A. 2013;110(26):10479-10486.

Figures

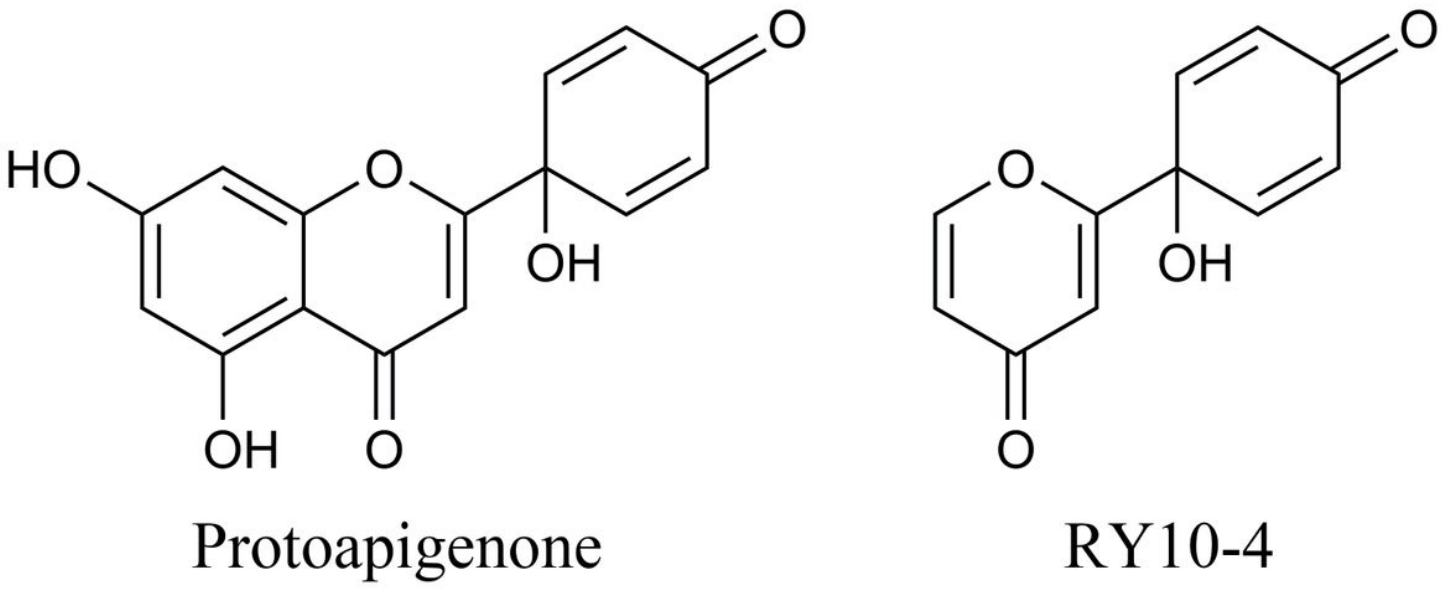

Figure 2

The structures of protoapigenone and RY10-4.

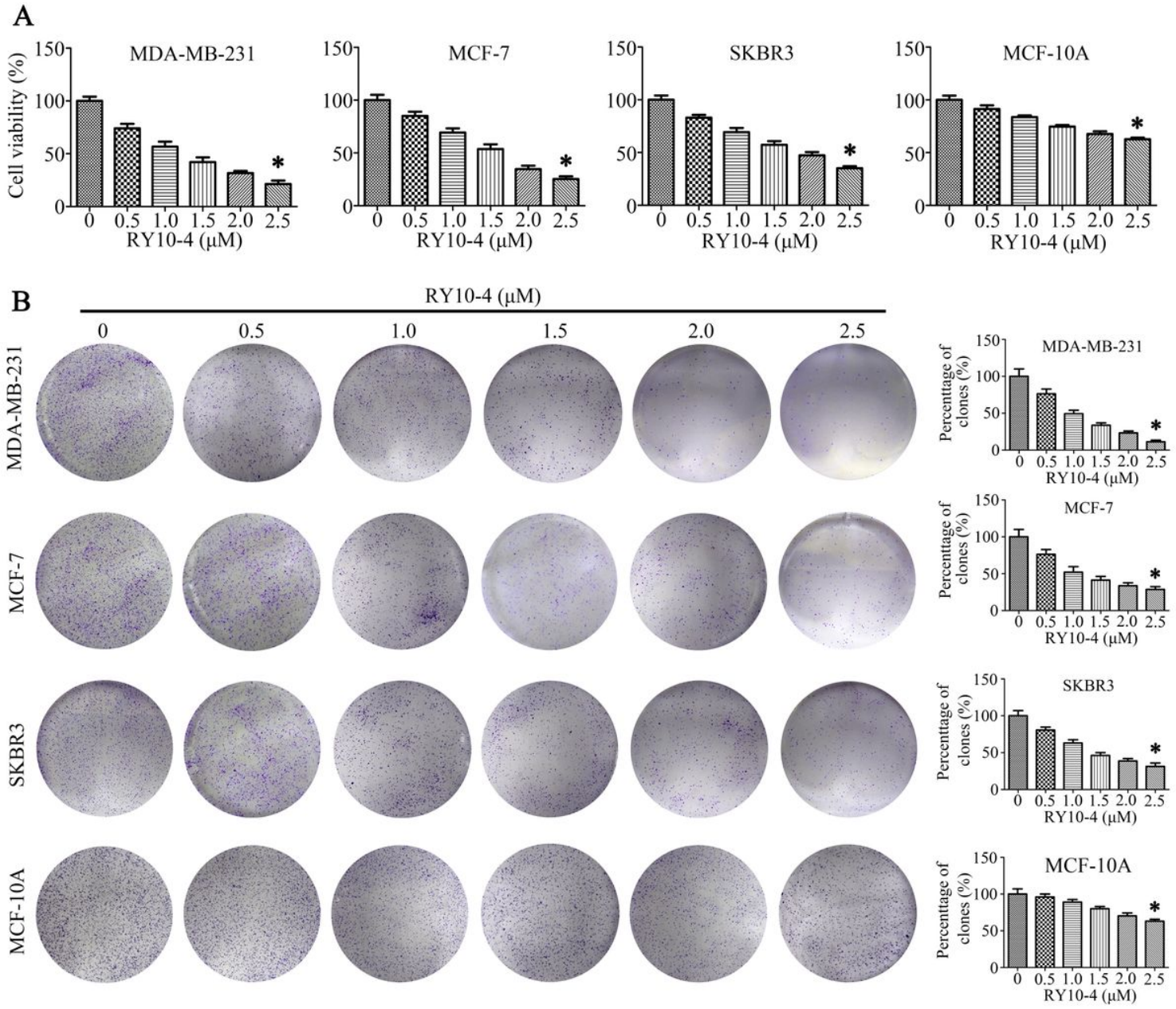

Figure 4

RY10-4 restrained proliferation of breast cancer cells. (A) Cell viability analysis of MDA-MB-231, MCF-7, SKBR3 and MCF10A cells treated by a concentration gradient of RY10-4. (B) Colony formation assay of MDA-MB-231, MCF-7, SKBR3 and MCF10A cells treated by a concentration gradient of RY10-4. *P < 0.05 vs control group (0 μM RY10-4).

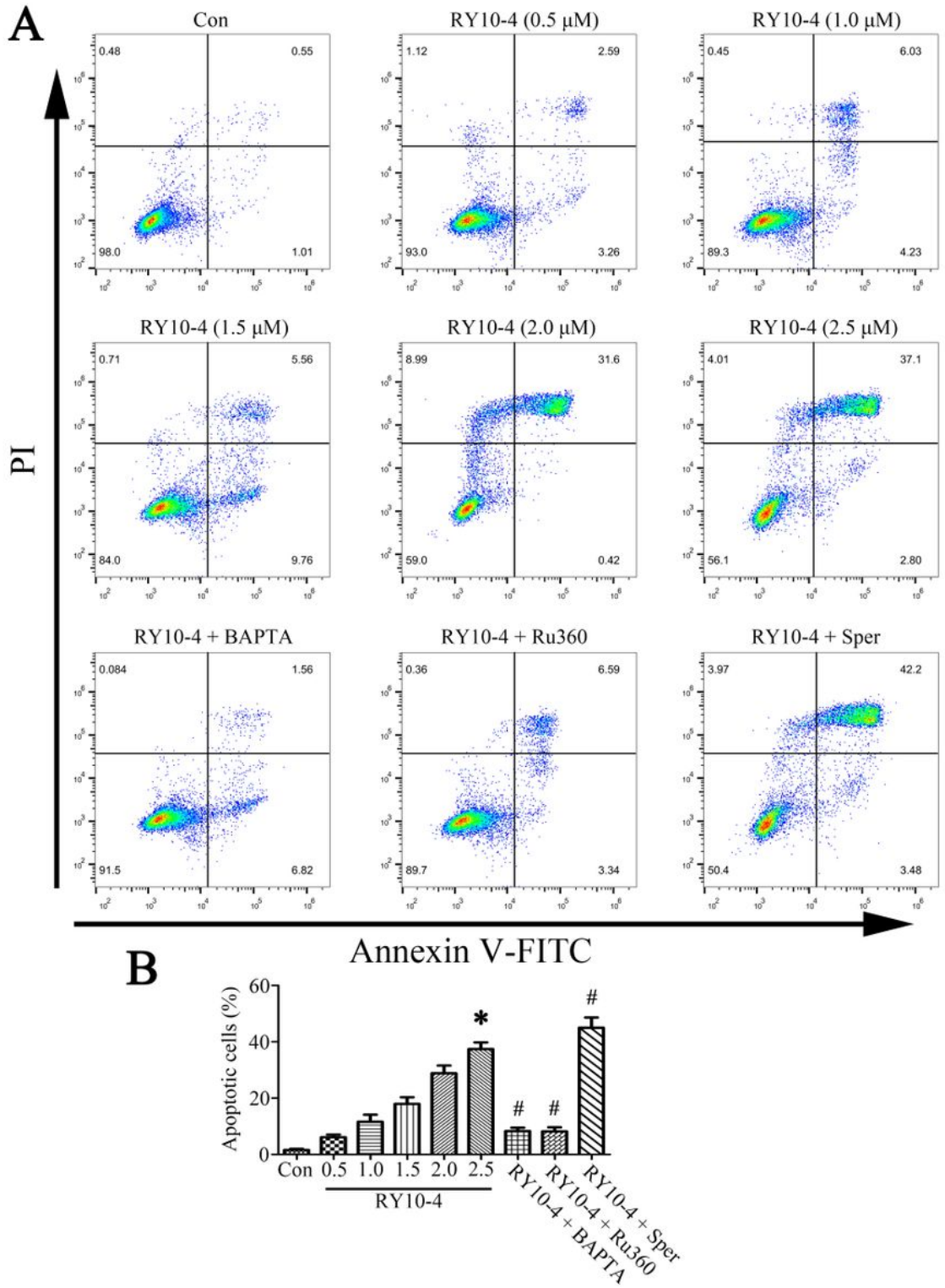

Figure 5

RY10-4 induced apoptosis of MDA-MB-231 cells. (A) Flow cytometry was performed to analysis the apoptosis of MDA-MB-231 cells with different treatments. (B) Statistical analysis of the flow cytometry results. *P < 0.05 vs control, #P < 0.05 vs RY10-4 (2.5 μM) group. Con, control; Sper, spermine.

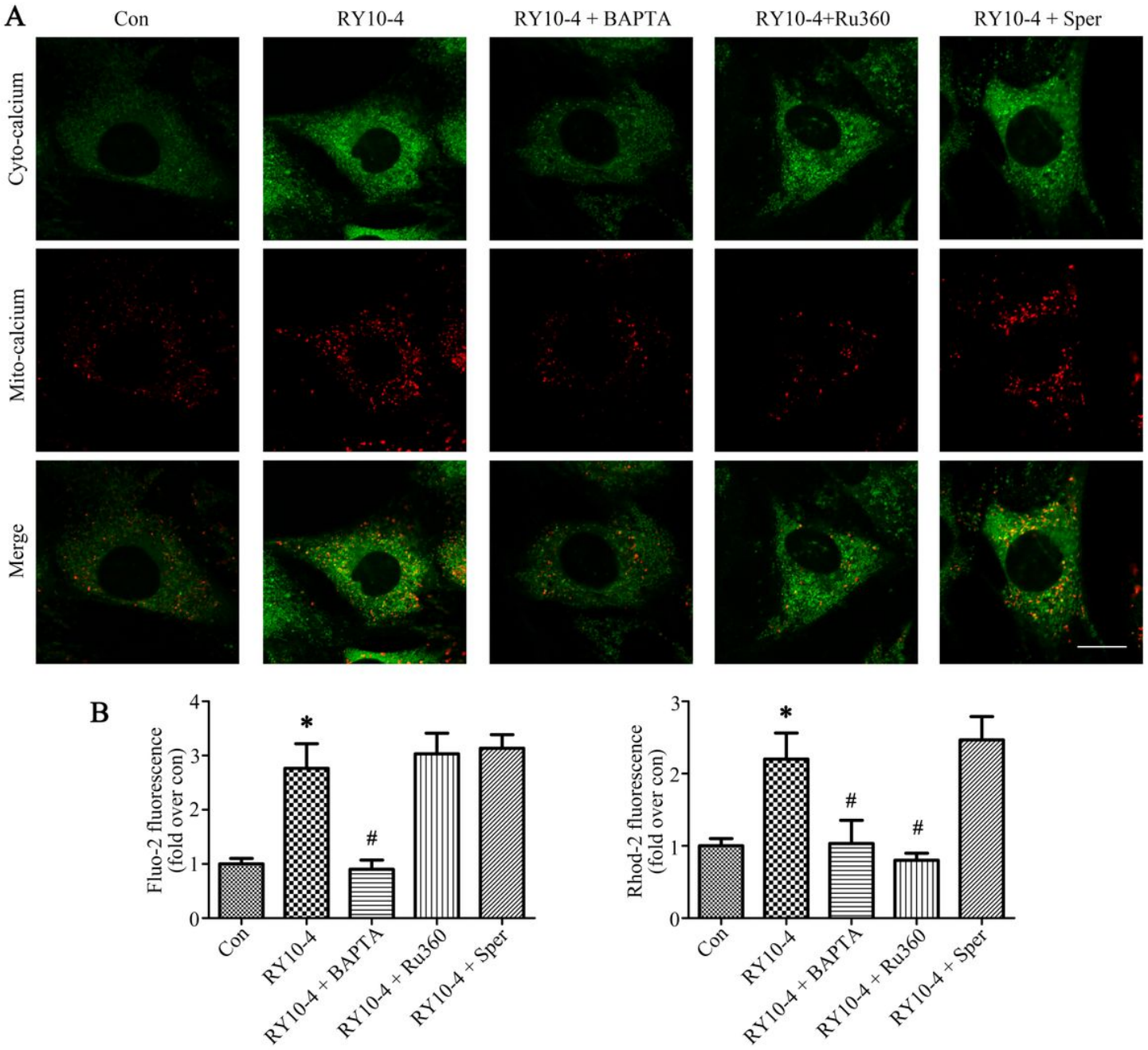

Figure 8

RY10-4 induced mitochondria Ca2+ overload and was reversed by Ru360. (A) Co-immunofluorescence of [Ca2+]c and [Ca2+]m. [Ca2+]c and [Ca2+]m were visualized by Fluo-2 and Rhod-2 probes respectively. Scale bar 10 μm. (B) Statistical analysis of the relative fluorescence intensity. *P < 0.05 vs control, #P < 0.05 vs RY10-4 (2.5 μM) group. Con, control; Sper, spermine.

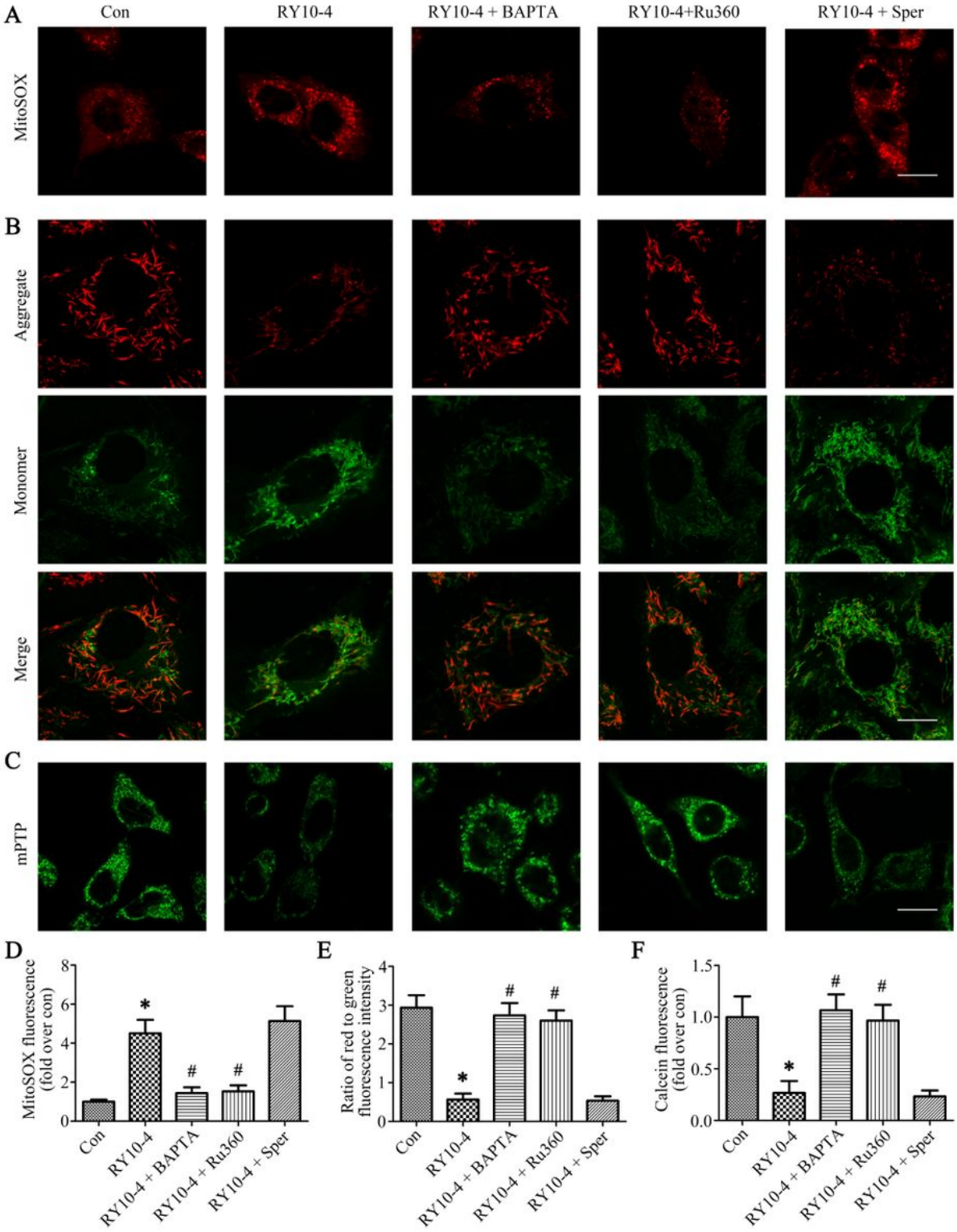

Figure 10

RY10-4 induced mitochondria dysfunction and was reversed by Ru360. (A, D) Mitochondrial O2•− was labeled by MitoSOX Red in MDA-MB-231 cells. Relative MitoSOX fluorescence was analysed. Scale bar 20 μm. (B, E) Determination of ΔΨm using the JC-1 probe. Red and green fluorescence represented the aggregate and monomeric form of JC-1 respectively. The merged images indicated co-localization of JC-1 aggregates and monomers. The ratio of red to green fluorescence intensity was calculated. Scale bar

10 μm. (C, F) mPTP activity in MDA-MB-231 cells was visualized by Calcein/AM after different treatments. Relative calcein fluorescence was analysed. Scale bar 20 μm. *P < 0.05 vs control, #P < 0.05 vs RY10-4 (2.5 μM) group. Con, control; Sper, spermine.

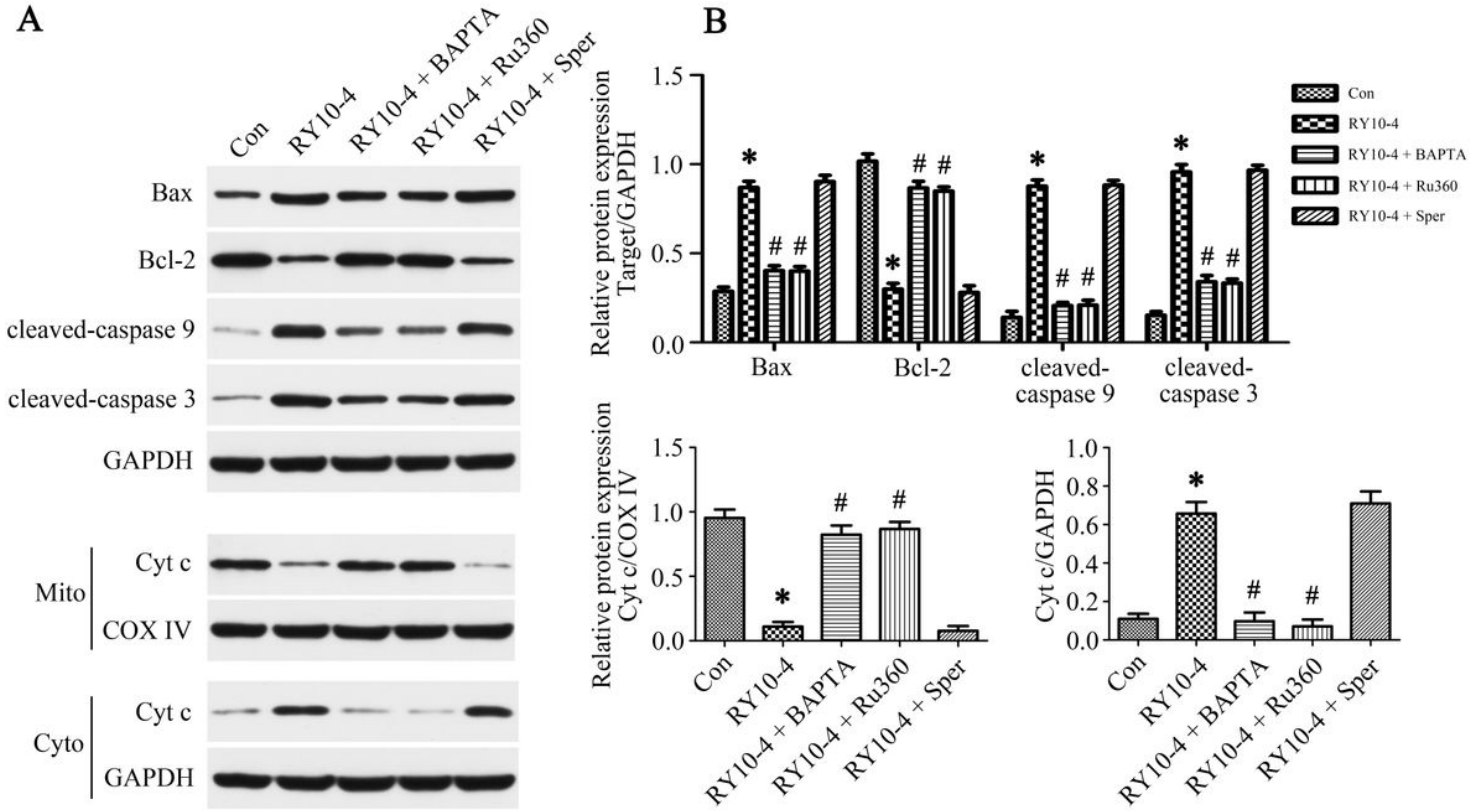

Figure 11

RY10-4 activated the mitochondria-mediated apoptosis in MDA-MB-231 and was reversed by Ru360. (A) Western blot analysis of the protein changes related to mitochondria-mediated apoptosis after different treatments. (B) Relative grey values analyses were performed. *P < 0.05 vs control, #P < 0.05 vs RY10-4 (2.5 μM) group. Con, control; Sper, spermine; Cyto, cytoplasm; Mito, mitochondria; Cyt c, cytochrome c.

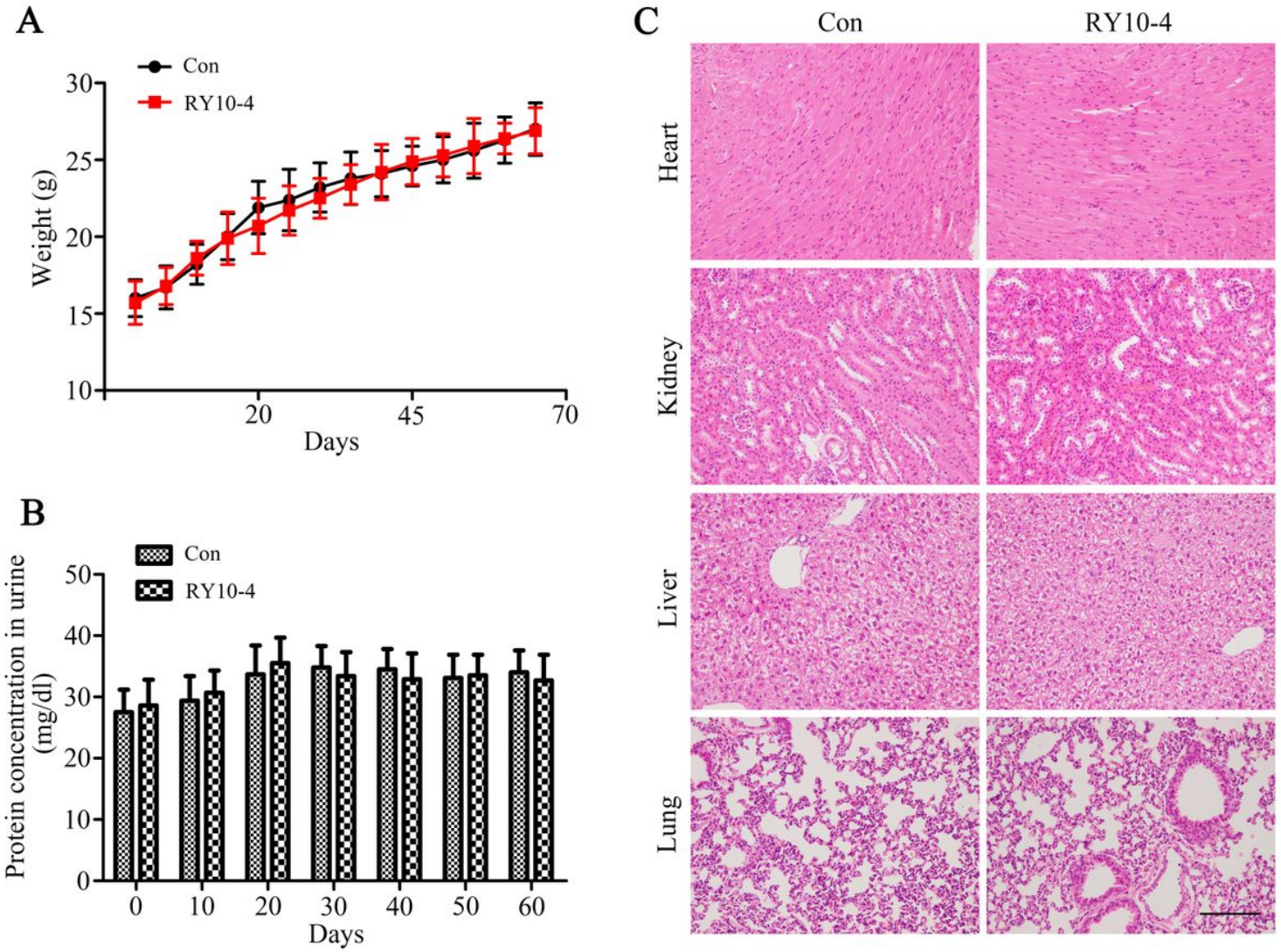

Figure 14

RY10-4 was well tolerated in animal models. (A) Weight of the mice in control and RY10-4 treatment (15 mg/kg, qod) group for a period of 65 days. (B) Protein urinalysis was carried out every 10 days for a period of 60 days. (C) Morphological observation of organs (hearts, kidneys, livers and lungs) in different groups by HE staining. Scale bar 50 μm. Con, control.

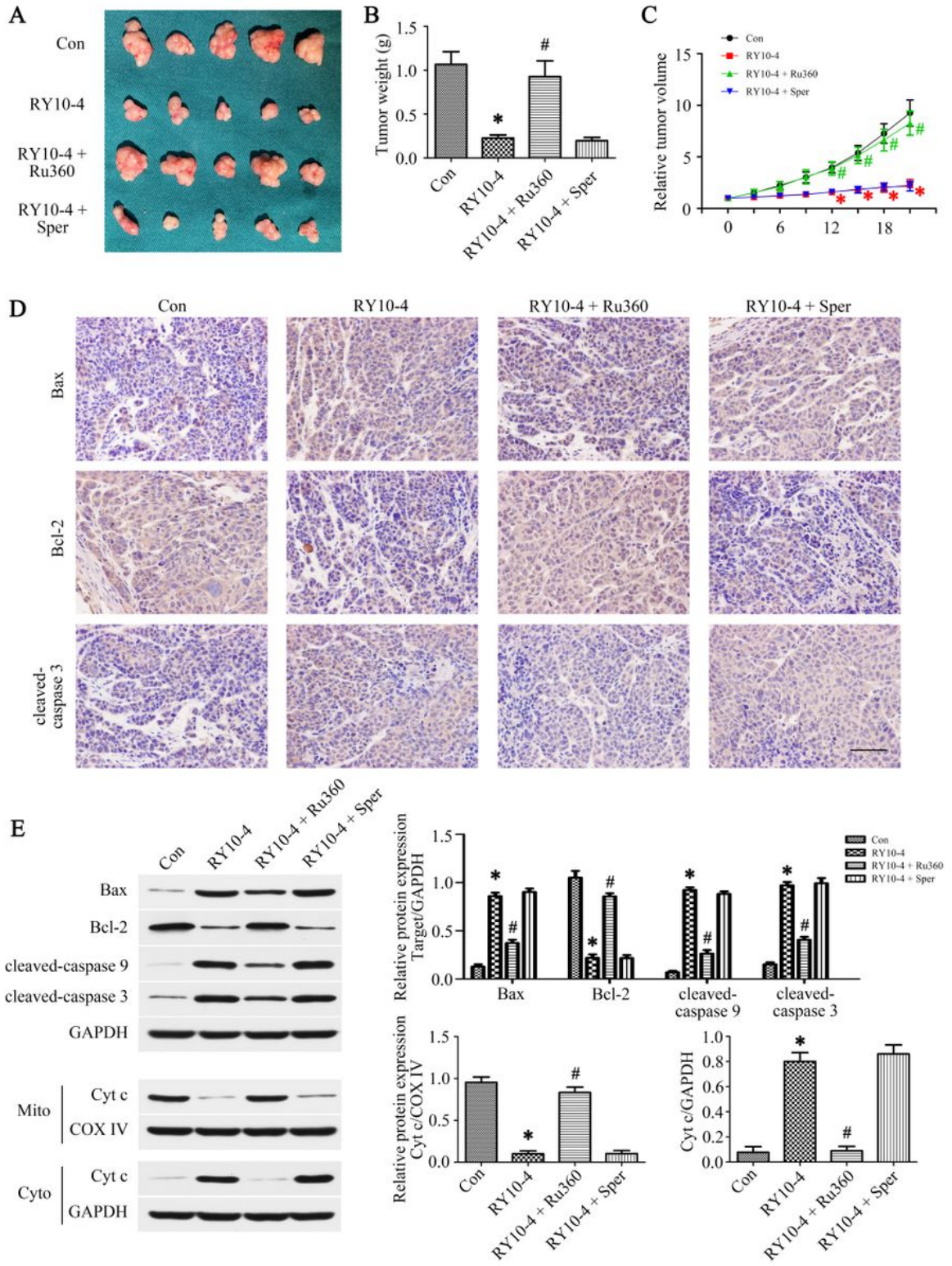

Figure 15

Ru360 reversed the inhibitory effect of RY10-4 on breast tumors in vivo. (A) Image of solid tumors obtained in each group after 3 weeks of treatment. (B) The weight of subcutaneous tumors was measured when mice were sacrificed after 3 weeks. (C) Relative tumor volume (RTV) in each group every 3 days for 3 weeks. (D) Immunohistochemistry analysis of Bax, Bcl-2 and cleaved-caspase 3 in each group. Scale bars, 50 μm. (E) Western blot analysis of the protein changes related to mitochondria-

mediated apoptosis in each group. Relative grey values analyses were performed. *P < 0.05 vs control, #P < 0.05 vs RY10-4 group. Con, control; Sper, spermine; Cyto, cytoplasm; Mito, mitochondria; Cyt c, cytochrome c.

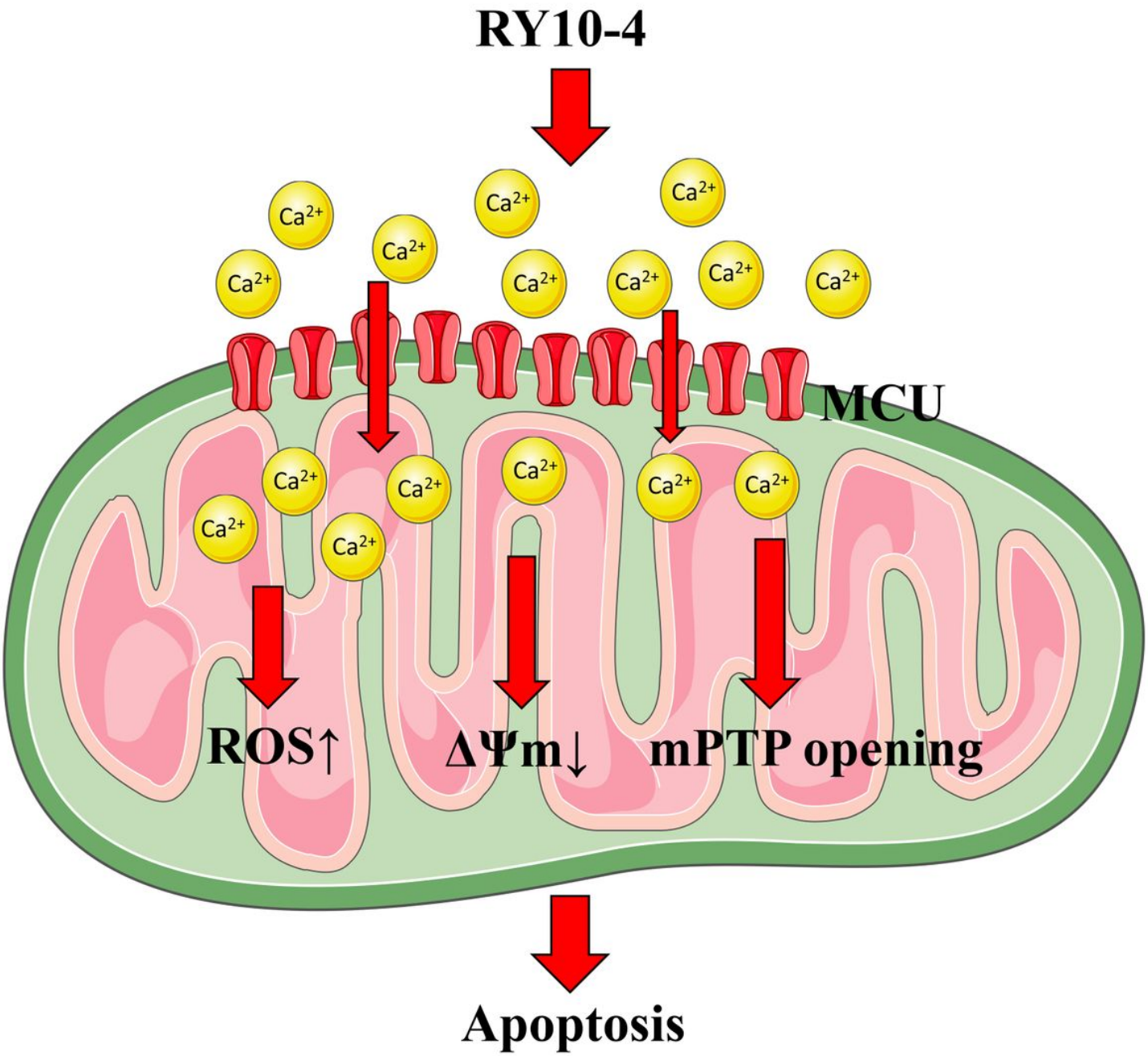

Figure 18

Graphical representation of the mechanism underlying the inhibitory effect of RY10-4 on breast cancer cells. RY10-4 induced mitochondrial Ca2+ influx through MCU, leading to mtROS accumulation, ΔΨm depolarization and mPTP opening, and finally triggered apoptosis of breast cancer cells.